

Timing and broad band spectroscopy of 1A 1118-61 with Suzaku

Chandreyee Maitra^{1,2*} Biswajit Paul^{1†} and Sachindra Naik^{3‡}

¹*Raman Research Institute, Sadashivnagar, Bangalore-560080, India*

²*Joint Astronomy Programme, Indian Institute of Science, Bangalore-560012, India*

³*Astronomy and Astrophysics Division, Physical Research Laboratory, Navrangapura, Ahmedabad-380009, Gujarat, India*

ABSTRACT

We present a timing and broad-band pulse phase resolved spectral analysis of the transient Be X-ray binary pulsar 1A 1118-61 observed during its outburst in January 2009 using *Suzaku* observations. *Suzaku* observations were made twice, once at the peak of the outburst, and once 13 days later at its declining phase. Pulse profiles from both observations exhibit strong energy dependence with several peaks at low energies and a single peak above ~ 10 keV. A weak, narrow peak is detected at the main dip of the pulse profiles from both observations in the energy bands below 3 keV, indicating the presence of a phase dependent soft excess in the source continuum. The broad-band energy spectrum of the pulsar could be fitted well with a partial covering cutoff power-law model and a narrow iron fluorescence line. We also detect a broad cyclotron feature at ~ 50 keV from both observations which is a feature common for accretion powered pulsars with high magnetic field strengths. Pulse phase-resolved spectral analysis shows an increase in the absorption column density of the partial covering component, as well as variation in the covering fraction at the dips of the pulse profiles, that naturally explains the energy dependence of the same. The cyclotron line parameters also show significant variation with pulse phase with a ~ 10 keV variation in the cyclotron line energy and a variation in depth by a factor of three. This can be explained either as the effect of different viewing angles of the dipole field at different pulse phases, or a more complex underlying magnetic field geometry.

Key words: X-rays: binaries– X-rays: individual: 1A 1118-61– stars: pulsars: general

1 INTRODUCTION

Be/ X-ray binaries are a subtype of neutron star high mass X-ray binaries (HMXBs) where the optical counterpart is a dwarf, subgiant or a giant O/Be star (luminosity class III-V) Reig (2011). These systems typically have a large orbital period, moderate eccentricity, and being a non-supergiant system, the Be star lies deep within the Roche lobe. X-ray emission is believed to be due to the accretion from the circumstellar disc of the rapidly rotating Be star onto the compact star. Most Be/ X-ray binaries are transient systems and display two types of outbursts such as (i) short, periodic, less luminous Type I outbursts ($L_x \leq 10^{36} - 10^{37} \text{ erg s}^{-1}$) lasting for a few days occurring at the phase of the periastron passage, and (ii) giant, longer, Type II outbursts ($L_x \geq 10^{37} \text{ erg s}^{-1}$) lasting for several weeks to months occurring when a large fraction of matter is accreted from the Be star's disk. Type II outbursts are sometimes followed by smaller recurrent type I outbursts.

Almost all Be/ X-ray binaries are accretion powered pulsars having a wide range of periods from seconds to hundreds of seconds. These are highly magnetized neutron stars accreting matter, channeling it along magnetic fields onto the magnetic poles, and forming an accretion column of X-ray emitting plasma on the neutron star surface (Pringle & Rees 1972; Davidson & Ostriker 1973; Gnedin & Sunyaev 1973; Lamb, Pethick & Pines 1973). The spectrum of these objects can be described by Comptonization of the soft X-rays by scattering in the hot plasma (Barnard & Arons 1981; Brainerd & Meszaros 1991; Meszaros & Nagel 1985a,b; Nagel 1981a,b). In the presence of such strong magnetic fields, photons undergo resonant scatterings by electrons in Landau levels to produce the Cyclotron Resonance Scattering Features (CRSF). These features have been found in more than 16 accretion powered pulsars (Mihara 1995; Coburn, Heindl & Rothschild 2002). The cyclotron line properties provide valuable information on the details of the emission, electron temperature, optical depth, and viewing geometries, and can map the magnetic field structure. For a brief review on the temporal and spectral properties of transient Be/X-ray binary pulsars, refer Paul & Naik (2011).

1A 1118-615 is a hard X-ray transient pulsar that was discovered with *Ariel V* in an outburst in 1974 (Eyles et al. 1975). The same series of observations revealed X-ray pulsations with a duration of 405.6 s (Ives, Sanford & Burnell 1975). The optical counter-

* E-mail: cmaitra@rri.res.in;

† E-mail: bpaul@rri.res.in;

‡ E-mail: snaik@prl.res.in

part (He 3-640=“WRA 793”) is a highly reddened Be star classified as an O9.5IV-Ve star (Chevalier & Ilovaisky 1975). It shows strong Balmer emission lines indicating the presence of an extended envelope (Motch et al. 1988). The distance to the source is estimated to be 5 ± 2 kpc from photometric and spectroscopic observations (Janot-Pacheco et al. 1981). *UV* observations (Coe & Payne 1985) reveal a P-Cygni profile in the C IV line which indicates a stellar outflow with a velocity of the order of 1600 ± 300 km s⁻¹. Coe & Payne (1985) also confirmed the magnitude of the companion and from the extinction value, the distance was suggested to be about 4 kpc. An orbital period of 24 ± 0.4 days was reported by Staubert et al. (2011). There have been three giant outbursts so far detected for this source. The first was in 1974 (Marashi et al. 1976). The second was detected in January 1992, and was observed by the Burst and Transient Source Experiment (*BATSE*) covering an energy range of 15 – 50 keV (Coe et al. 1994; Marashi et al. 1976). The outburst lasted for ~ 30 days and pulsations with a period ~ 406.5 s were detected up to 100 keV (Coe et al. 1994). The same work also reported a spin change rate of -0.016 s/day at the decay of the outburst.

The source remained in quiescence for 17 years until 4 January 2009 when a third outburst was detected by *Swift* (Mangano 2009). Pulsations were detected at ~ 407.68 s with the pulse profile showing a complex structure. The complete outburst was regularly monitored with *RXTE* (Rossi X-ray Timing Explorer). *INTEGRAL* detected a flaring activity in the source ~ 30 days after the main outburst (Leyder et al. 2009). *Suzaku* observed the source twice, once at the peak of the outburst and once 13 days later. *RXTE* observations of the source was analyzed by Doroshenko et al. (2010) who presented the broad-band spectrum, and reported the presence of a broad prominent absorption feature at ~ 55 keV which they interpreted as a CRSF. Detailed timing and spectral analysis of the same set of observations was reported by Devasia et al. (2011a) which included the energy dependence of the pulse profiles and pulse phase-resolved spectroscopy of the continuum spectra. They also detected quasi-periodic oscillations (QPO) at 0.07-0.09 Hz which showed a significant energy dependence. Analysis of the same *Suzaku* observations was reported by Suchy et al. (2011) which confirmed the presence of the CRSF at ~ 55 keV. They also performed pulse phase-resolved spectroscopy for three different pulse phases *i.e.* the two peaks and the minimum of the pulse profile. Suchy et al. (2011) thus reported a change in the continuum parameters like the photon index and high energy cutoff, and also the centroid energy in the three above mentioned phases.

The pulse profiles of 1A 1118-615 show multiple energy dependent dips. Dips in the

pulse profiles can be naturally produced by absorption in the accretion stream that is phase locked with the neutron star. This had been explored for GX 1+4 (Galloway et al. 2001), RX J0812.4-3114 (Corbet & Peele 2000), 1A 1118-61 (Devasia et al. 2011a), GX 304-1 (Devasia et al. 2011b) with *RXTE*, KS 1947+300 (Naik et al. 2006) with *Beppo-Sax*, and GRO J1008-57 with *Suzaku* (Naik et al. 2011). Suchy et al. (2011) did include a phase dependent additional absorption component in their analysis but did not probe the narrow dips of the pulse profiles, as they carried out phase resolved analysis by dividing the pulse profile into only three phase bins. Devasia et al. (2011a) used *RXTE-PCA* (*RXTE* Proportional Counter Array) data covering a limited energy-band. We report here a more comprehensive timing and broad-band spectral analysis of *Suzaku* observations of 1A 1118-61 during the 2009 outburst. We have probed the energy dependence of the pulse profiles in more detail and have carried out pulse phase-resolved spectroscopy in narrow phase bins to explain its complex nature.

We have also carried out pulse phase-resolved spectroscopy of the cyclotron absorption feature in this source and obtained one of the most detailed pulse phase-resolved information available for CRSF till date. In addition, we have detected a narrow phase dependent soft excess peak in both observations of this source. In section 2, we describe details of the observations and data reduction. In section 3, we describe the timing analysis including the energy dependence of the pulse profiles and the power density spectra. In section 4, we present the pulse phase averaged and pulse phase-resolved spectroscopy of the *Suzaku* observations followed by discussions & conclusions in section 5.

2 OBSERVATIONS & DATA REDUCTION

The hard X-ray transient pulsar 1A 1118-61 was observed with *Suzaku*, once at the peak of the outburst and once in its decline 13 days later. Figure 1 shows the one day averaged long-term light curve of 1A 1118-61 using data from the the All Sky Monitor (ASM) (1.5–12 keV) onboard *RXTE* and from the *Swift*-BAT all sky monitor (15 – 50 keV)¹. The arrow marks in the figure shows the *Suzaku* observations of the pulsar during the 2009 outburst *Suzaku* (Mitsuda et al. 2007), covers the 0.2-600 keV energy range. It has two sets of instruments, the X-ray Imaging Spectrometer XIS (Koyama et al. 2007) covering the 0.2-12 keV range,

¹ See <ftp://heasarc.gsfc.nasa.gov/xte/data/archive/ASMPProducts/> and <http://heasarc.nasa.gov/docs/swift/results/transients/> for details

the Hard X-ray Detector (HXD) having PIN diodes (Takahashi et al. 2007) covering the energy range of 10–70 keV, and GSO crystal scintillators detectors covering the 70–600 keV energy band. The XIS consists of four CCD detectors, three of them are front illuminated (FI) and one is back illuminated (BI).

We have used the data processed with *Suzaku* data processing pipeline ver. 2.3.12.25. The observations carried out on 15 January 2009 (Obs. ID–403049010; hereafter quoted as Obs-1) has an useful exposure of 49.7 ks and that on 28 January 2009 (Obs. ID–403050010; hereafter quoted as Obs-2) has an useful exposure of 44.2 ks. In both observations, the source was observed at ‘HXD nominal’ pointing position ². The XIS was operated in ‘standard’ data mode in the ‘ $\frac{1}{4}$ window’ option which gave a time resolution of 2 s.

For extracting the XIS and HXD/PIN light curves and spectra, we used cleaned event data. The cleaned events of the XIS data were screened for standard criteria ³. We extracted the XIS light curves and spectra from these cleaned events by selecting a circular region of 3′ around the source centroid. The XIS count rates for Obs-1 and Obs-2 were 44.5 c/s and 8.5 c/s, respectively. We also extracted the background light curves and spectra by selecting a region of the same size 18′ away from the source centroid. Response files and effective area files were generated by using the FTOOLS task ‘xisresp’. For HXD/PIN background, simulated ‘tuned’ non X-ray background event files (NXB) corresponding to January 2009 were used to estimate the non X-ray background⁴, and the cosmic X-ray background was simulated as suggested by the instrument team⁵ applying appropriate normalizations for both cases. Response files of the respective observations were obtained from the *Suzaku* Guest Observer Facility.⁶

Observations of a bright source like 1A 1118-61, especially at the peak of the outburst should be checked for possible effects of pileup. Suchy et al. (2011) had applied the tool ‘pile_estimate.sl’ to estimate the pileup fraction in XIS and had excluded regions of the CCDs with pileup fraction above 5%. We checked for the effect of pileup for Obs-1 by extracting spectra with the central 10″ and 15″ radii removed, and generated their corresponding responses. Comparing these two spectra with the original spectrum, we observe that the spectral shape remains almost the same in all the cases and the change in photon index

² See <http://heasarc.gsfc.nasa.gov/docs/suzaku/analysis/abc/> website for more information on instruments

³ See <http://heasarc.nasa.gov/docs/suzaku/analysis/abc/node9.html> for standard screening criteria

⁴ <http://heasarc.nasa.gov/docs/suzaku/analysis/pinbgd.html>

⁵ http://heasarc.nasa.gov/docs/suzaku/analysis/pin_cxb.html

⁶ <http://heasarc.nasa.gov/docs/heasarc/caldb/suzaku/> and used for the HXD/PIN spectrum

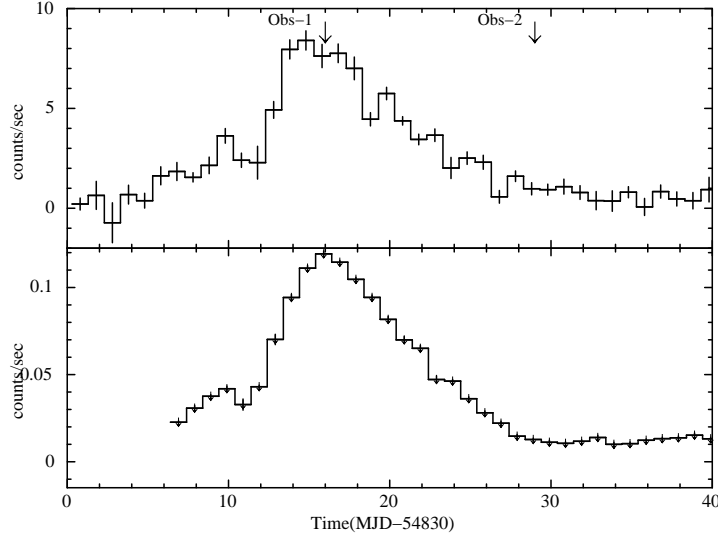


Figure 1. The top panel shows the one day binned *RXTE*-ASM (1.5-12 keV) light curve of 1A 1118-61, the bottom panel shows the one day binned light curve from the *Swift*-BAT all sky monitor (15-50 keV). The arrows in the top panel indicate the time of the *Suzaku* observations of 1A 1118-61.

is only ~ 0.02 for the XISs, where this effect is the most pronounced for XIS-3. Hence, our results are not expected to vary significantly due to this effect, since our main focus is on variations of the spectral parameters with pulse phase that is much larger than this difference. Obs-2, being an order of magnitude fainter than Obs-1 does not require this check.

3 TIMING ANALYSIS

3.1 Pulse profiles

For the timing analysis, we applied barycentric corrections to the event data files using the FTOOLS task 'aebarycen'. Light curves with a time resolution of 2 s and 1 s were extracted from the XIS (0.2–12 keV) and the HXD/PIN (10–70 keV), respectively. We searched for pulsations in both observations by applying pulse folding and χ^2 maximization technique. The pulse period was found to be 407.49 ± 0.73 s for Obs-1 (MJD 54846) and 407.40 ± 0.40 s for Obs-2 (MJD 54859) respectively. We created energy resolved pulse profiles by folding the light curves in different energy bands with the respective pulse periods. Light curves from the three XISs were added together to create the pulse profiles in the 0.2–12 keV energy range. The pulse profiles are found to have complex energy dependent structures on both the days, with more than one peak in the XIS energy band, and a single peaked but asymmetric structure in the PIN energy band, as shown in Figures 2 & 3. In Obs-1 (Figure 2), the profiles show a double peaked structure at lower energies (less than 12 keV). The

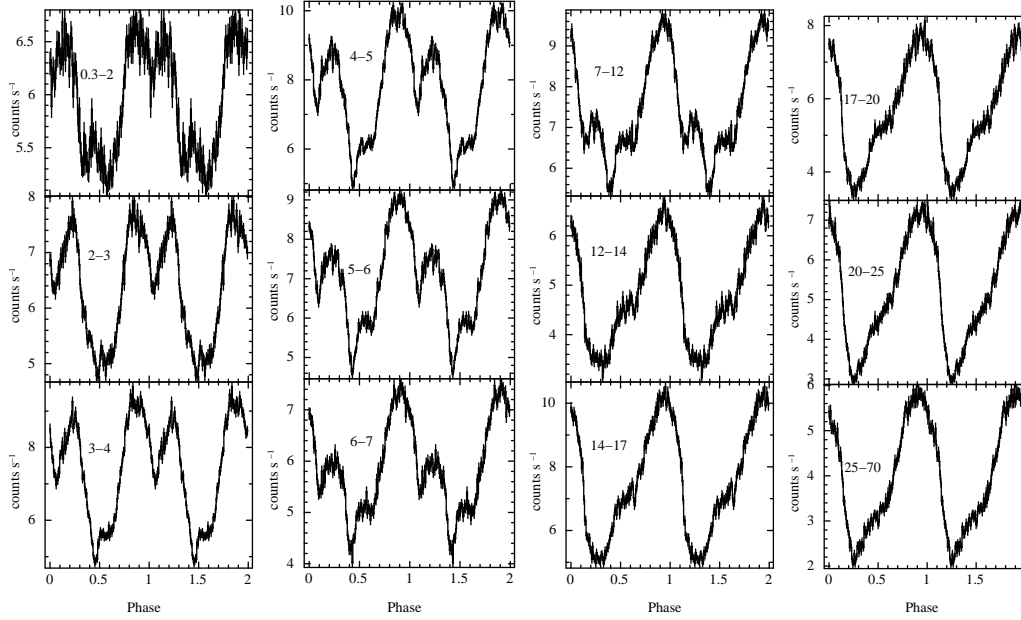


Figure 2. Energy dependent pulse profiles of 1A 1118-61 using the XIS and PIN data for Obs-1. Captions inside the figure (in units of keV) represent the energy range for which the profiles were created. The pulse profiles in the 0.2–12 keV energy range are made from the XIS data (data from all the three XISs are added together), where as profiles in the 12–70 keV range are obtained from the PIN data.

secondary peak (phase ~ 0.2) decreases in strength with energy and disappears at ~ 12 keV. At high energies (greater than 12 keV), the profile shows a single peaked structure with a large pulse fraction. A narrow low energy peak (less than 2 keV) is seen coincident with the pulse minima at higher energies (phase ~ 0.46). For Obs-2 (Figure 3), one main peak (phase ~ 0.5) is seen at all energy bands, which is narrow and symmetric at low energies (less than 3 keV). The main peak gets broadened up to 12 keV, and becomes a broad asymmetric pulse at higher energies. A narrow and weaker peak (at phase ~ 0.2) appears at energies greater than 2 keV before the main peak. At higher energies (greater than 12 keV), this feature gradually merges with the rising part of the main peak. Another pulse component (phase ~ 0.75) is seen after the main peak only in the energy band below 2 keV and 6–7 keV. The pulse profiles show a single asymmetric peaked structure in the energy ranges greater than 12 keV with the pulse minima at phase ~ 0.8 . The pulse profiles show the presence of an additional peak at phase ~ 0.96 in the lowest energy bin (0.3–2 keV). The complex energy dependence of the pulse profile implies significant changes in the energy spectrum with the pulse phase, and also a complex underlying spectrum. A detailed discussion is presented in section 5.1.

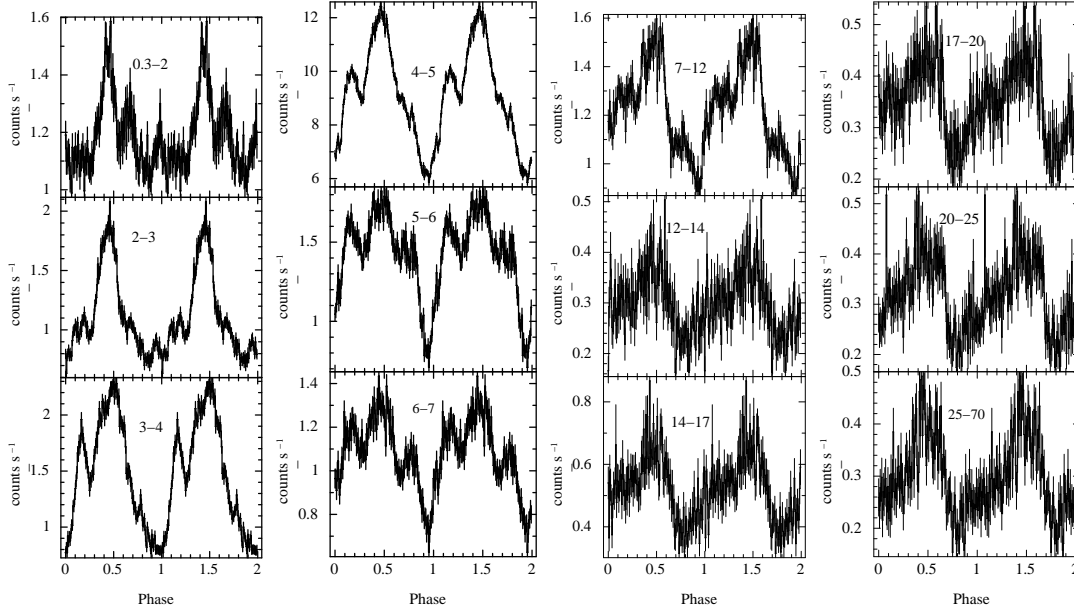


Figure 3. Same as Figure 2 for Obs-2.

3.2 Power Density Spectra

We created the Power Density Spectra (PDS) using the FTOOL task '*powspec*' from the XIS light curves (0.2-12 keV) which was divided into segments of 4096 s with a time resolution 2 s. The PDS obtained from all these segments were rebinned with a geometric rebinning factor, and were averaged to produce the final PDS. The average PDS was also normalized such that its integral gave the squared rms fractional variability and expected white noise level was subtracted. The PDS from both observations clearly shows the peak at ~ 0.0025 Hz corresponding to the spin frequency, with its harmonics visible at higher frequencies. Obs-1 shows a quasi-periodic oscillation (QPO) feature at 0.087 ± 0.008 Hz.

We fitted the PDS with a power-law component corresponding to the continuum by avoiding the peaks corresponding to the spin frequency and its harmonics. The QPO feature was fitted with a Gaussian function, giving a detection significance of 13σ , quality factor ($\nu/FMHM$) of 4.2 ± 0.4 and the rms fractional variability of 4.58 ± 0.17 % in the 0.2–12 keV energy range of XIS. Obs-2 shows a broad feature at 0.026 ± 0.003 Hz. We have fitted the feature with a Gaussian function which gave a detection significance of 7σ , quality factor of 1.70 ± 0.2 and rms value of 7.93 ± 0.58 %. The energy dependence of the QPO has been investigated for Obs-1. Multiple PDS were extracted for seven different energy ranges between 3 and 10 keV, each with a width of 1 keV in the XIS energy band. The rms of the QPO feature shows an increase from 4.09% to 7.74% in the XIS energy range. Figure 4 shows the PDS for both observations in the energy band of 0.2–12 keV. We note here that it is quite unusual to

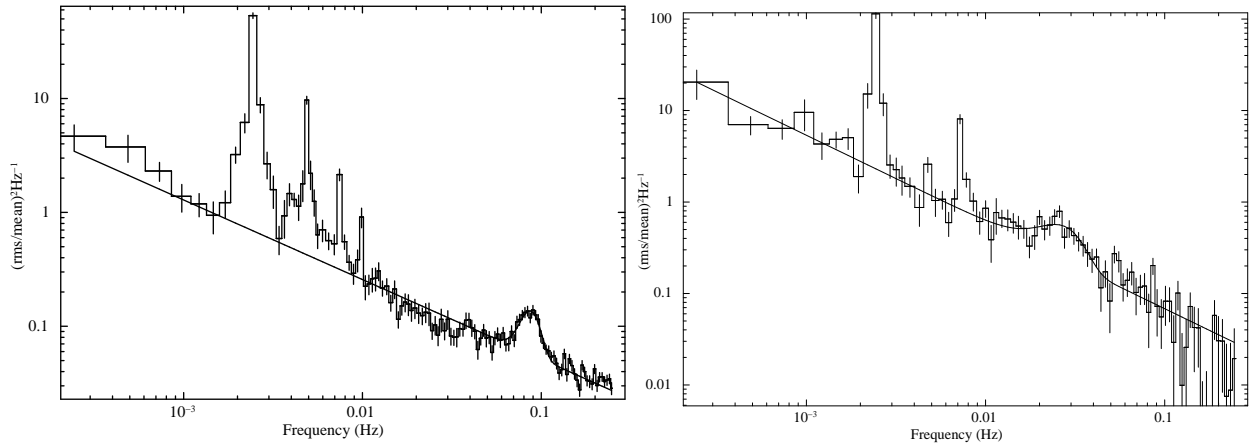


Figure 4. Average PDS of 1A 1118-61 for both observations showing the QPO feature in the energy band of 0.2–12 keV. The left panel shows the PDS for Obs-1 and the right panel shows the same for Obs-2. In both the figures, the spin period at 0.0025 Hz and its harmonics are clearly seen with the QPO at 0.087 Hz visible for Obs-1 and the broad feature at 0.026 Hz visible for Obs-2.

detect QPOs with imaging spectrometer detectors. In this source we have not only detected the QPOs, but are also able to investigate its energy dependence.

4 SPECTRAL ANALYSIS

4.1 Pulse phase averaged spectroscopy

The continuum emission from HMXB accretion powered pulsars can be interpreted as Comptonization of soft X-rays in the plasma above the neutron star surface. It can be modelled as a power-law with an exponential cutoff or as a broken power-law (White, Swank & Holt 1983; Mihara 1995; Coburn, Heindl & Rothschild 2002).

In the presence of strong magnetic fields, the continuum photons produced inside the hot region by thermal bremsstrahlung and Comptonization may get resonantly scattered in the line forming regions, producing a cyclotron resonant scattering feature (CRSF). Often a strong narrow Fe $K\alpha$ line can also be found originating from the cold dense matter in the vicinity of the neutron star.

We performed pulse phase averaged spectral analysis of 1A 1118-61 using spectra from the front illuminated CCDs (XISs-0 and 3), back illuminated CCD (XIS-1), and the PIN. Spectral fitting was performed using *XSPEC* v12.6.0. The energy ranges chosen for the fits were 0.8–10 keV for the XISs, and 10–70 keV for the PIN spectra. We neglected the 1.75–2.23 keV energy range in order to take out the artificial structures in the XIS spectra at around the Si edge and Au edge. After appropriate background subtraction we fitted the spectra simultaneously with all the parameters tied, except the relative instrument normalizations

which were kept free. The XIS spectra were rebinned by a factor of 5 from 0.8–6 keV and 7–10 keV. However due to the presence of a narrow iron line, the spectrum was rebinned only by a factor of 2 in the 6–7 keV energy range. The PIN spectra were rebinned by a factor of 3 in the 10–70 keV range. We had initially tried to fit the continuum with a partial covering high-energy cutoff model (similar modeling for this source has been done in Devasia et al. (2011a)) which gave a very low value of high-energy cutoff ($\sim 0\text{--}3$ keV) for some of the phase bins while performing pulse phase resolved spectroscopy described later in section 4.2. High energy cutoff in this scenario is equivalent to the cutoff power-law model. Hence we fitted the broad band energy spectrum of 1A 1118-61 with a partial covering cutoff power-law model with an interstellar absorption and a gaussian line for an Fe $K\alpha$ feature at 6.4 keV. In addition, a broad cyclotron absorption feature was also found in the spectra at 49 ± 0.5 keV in Obs-1 and $52^{+4.9}_{-3.1}$ keV in Obs-2. This feature was fitted with the *XSPEC* standard model ‘cyclabs’ which is a cyclotron absorption line having a Lorentzian profile. Presence of the broad cyclotron feature at ~ 55 keV had already been reported from *RXTE* observations (Doroshenko et al. 2010) and from these *Suzaku* observations (Suchy et al. 2011). The analytical form of the model which was used to fit the spectra is as follows:

$$F(E) = \exp^{-\sigma(E)N_{H1}} ((N1 + N2 e^{-\sigma(E)N_{H2}}) * CYABS(E) + G) I(E) \quad (1)$$

Where CYABS is the Lorentzian cyclotron line profile given by

$$CYABS(E) = \exp[-D_{Cycl} \frac{(W_{Cycl}E/E_{Cycl})^2}{(E - E_{Cycl})^2 + W_{Cycl}^2}] \quad (2)$$

where E_{Cycl} is the energy of the cyclotron line & D_{Cycl} & W_{Cycl} are the depth and width of the cyclotron line. $I(E)$ can be expressed as

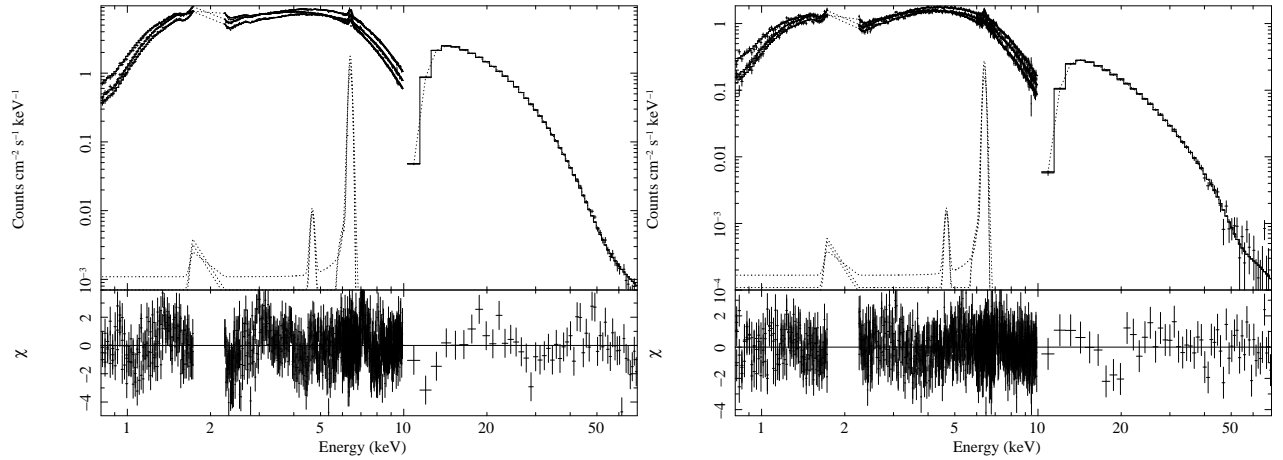
$$I(E) = E^{-\Gamma} \exp(\frac{-E}{\beta}) \quad (3)$$

Where Γ is the power-law photon index and β is the e-folding energy of the exponential roll-over in keV. $N1$ and $N2$ are the normalizations of the two power-laws. N_{H1} is the Galactic hydrogen column density along our line of sight, and N_{H2} is the column density of the material that is local to the neutron star. σ is the photo-electric cross-section and G is the gaussian line energy. Thus the covering fraction of the more absorbed power-law is given by $Cv_{fract} = \frac{N2}{N1+N2}$.

Spectral fitting showed that Obs-1 was softer than Obs-2. Since the energy spectrum had a strong pulse phase dependence, we did not expect the pulse averaged spectra to fit well to a simple continuum model. The best-fit had a reduced χ^2 of 1.79 for 1022 degrees of

Table 1. Best fitting spectral parameters of 1A 1118-61. Errors quoted are for 90 per cent confidence range.

Parameter	15 January (Obs-1)	28 January (Obs-2)
N_{H1} (10^{22} atoms cm^{-2})	0.86 ± 0.01	$0.61^{+0.01}_{-0.02}$
N_{H2} (10^{22} atoms cm^{-2})	$14.25^{+0.71}_{-0.59}$	$7.78^{+0.14}_{-0.24}$
Cv_{fract}	0.24 ± 0.01	0.73 ± 0.01
PowIndex (Γ)	0.37 ± 0.02	$0.97^{+0.02}_{-0.04}$
E-folding energy β (keV)	$21.6^{+0.7}_{-0.6}$	$24.8^{+1.6}_{-2.4}$
E_{Cycl}	$49.3^{+0.5}_{-0.5}$	$51.9^{+4.9}_{-3.1}$
D_{Cycl}	1.70 ± 0.05	$1.00^{+0.5}_{-0.3}$
W_{Cycl}	19.2 ± 1.1	$10.7^{+3.5}_{-2.5}$
Iron line energy (keV)	6.40 ± 0.01	6.40 ± 0.01
Iron line eqwidth (eV)	51.0 ± 1.5	41.9 ± 4.0
Flux (XIS) (0.8-10 keV) ^a	2.45 ± 0.01	0.45 ± 0.04
Flux (PIN) (10-70 keV) ^b	1.02 ± 0.01	0.11 ± 0.04
reduced χ^2 /d.o.f	1.79/1022	1.21/1023

^a Flux is in units of 10^{-9} ergs $cm^{-2}s^{-1}$ ^b Flux is in units of 10^{-8} ergs $cm^{-2}s^{-1}$ **Figure 5.** The pulse-phase averaged spectrum of 1A 1118-61 at the peak of the outburst (Obs-1; left panel) and at the decline (Obs-2; right panel), using XIS from 0.8–10 keV and PIN from 10–70 keV. The upper panel shows the best-fit spectra along with the model components. The residuals are given in the bottom panels.

freedom and 1.21 for 1023 degrees of freedom for Obs-1 and Obs-2, respectively. Table 1 shows the best-fit parameters for the model. Figure 5 shows the best-fit spectra along with the residuals for both observations.

4.2 Pulse phase-resolved spectroscopy

The strong energy dependence of the pulse profiles, as shown in Figures 2 & 3 implies a dependence of the energy spectrum on the pulse phase. To investigate this, we performed pulse phase-resolved spectroscopy by dividing the data into 25 phase bins, applying phase filtering in the FTOOLS task XSELECT. Plotting the ratio of the spectra at some interesting phases, like the pulse peaks and dips to the phase average spectrum can clearly bring out the complexity of the spectral changes with pulse phase. In Figures 6 & 7, we plot the ratio

of few of the pulse phase-resolved spectra with the pulse phase averaged spectrum for both observations. For phase-resolved spectral analysis, For phase-resolved spectral analysis, we used same background spectra and response matrices for the XIS and PIN data as was used in the case of phase averaged spectroscopy. We fitted the spectra in the same energy ranges and rebinned them by the same factor as in the phase averaged case for the XIS spectra. For the PIN spectra however, we rebinned Obs-1 by the same factor as the phase averaged spectra, but rebinned Obs-2 with a higher rebinning factor of 8 above 40 keV due to poor statistics. The value of N_{H1} and the iron line width were fixed to the corresponding phase averaged values (as given in Table 1). Due to limited statistics in the PIN energy range, we could not vary all the three parameters of the 'cyclabs' model simultaneously and hence fixed the cyclotron width to its phase averaged value. At the main dip of the pulse profiles, an additional peak at the lowest energy (less than 2 keV) was apparent in the spectra of both observations, that indicate a soft excess and an additional blackbody component was required to fit the spectra for those phase ranges. For Obs-1, the phase bin corresponding to 0.40–0.44 required an additional blackbody component with a temperature $kT=0.47$ keV. Obs-2 on the other hand required a blackbody with a temperature $kT=0.34$ keV in the phase bin of 0.96–1.00. The radius R_{bb} of the region from which this soft-excess is emitted can be calculated as

$$\frac{L_{bb}}{4\pi R_{bb}^2} = \sigma T_{bb}^4$$

Where L_{bb} is the blackbody luminosity and T_{bb} the corresponding temperature. The radius of the blackbody emitting region determined from Obs-1 and Obs-2 are ~ 6 km and 4 km respectively. The reduced χ^2 for the phase-resolved spectroscopy were in the range of 1.03-1.46 and 1.32-2.5 for 1024 degrees of freedom, for Obs-1 and Obs-2 respectively. The variation of the spectral parameters with pulse phase are shown in Figure 8. The results obtained from the pulse phase resolved spectroscopy as seen in this figure are summarized below:

Obs-1 : There was an abrupt increase in the absorption column density (N_{H2}) in the narrow dip of the profile at phase ~ 0.1 although the covering fraction (Cv_{fract}) remained small. In the main dip of the profile at pulse phase of ~ 0.5 , both the covering fraction and the N_{H2} value increased. Spectral hardening was observed in both the peaks of the pulse profile.

Obs-2 :

The covering fraction remained nearly constant at a high value of ~ 0.8 throughout the pulse phase indicating a more or less symmetric distribution of material around the neutron

star. The value of N_{H2} increased dramatically at the main dip (phase ~ 0.9), although the covering fraction decreased to ~ 0.5 . In the phase range ~ 0.5 – 0.7 in Obs-2, no high-energy cutoff was required to fit the spectra. The reason for this is not very clear.

For both observations, the power-law continuum parameters like the power-law index (P_{index}), normalization (P_{norm}), and the cutoff energy (E_{cut}) varied significantly with the pulse phase.

Phase resolved spectroscopy of the cyclotron line feature:

The high energy part (greater than 40 keV) of the data of Obs-1 had enough statistics to investigate the variation of cyclotron energy and depth as a function of phase. Instead of varying all the three cyclotron parameters, we fixed the cyclotron width to the phase averaged value. To perform phase-resolved spectroscopy of the cyclotron feature, 25 phase bins were used for the XIS data as in the previous cases. Due to limited statistics in the PIN data, pulse phase resolved PIN spectra with phases centered at the XIS phase bins were generated but at thrice their widths, resulting in 25 overlapping phase bins out of which only 8 were independent. Figure 9 shows the variation of the cyclotron energy and depth with phase. There is an indication of anti-correlation or a phase shift between the energy and the depth of the CRSF feature. The cyclotron energy shows a variation of about 10 keV and has two peaks at the same phase of the pulse peaks in the XIS energy band. As is also evident from Figure 9, The depth of the CRSF also shows a double peaked structure with large variation by a factor of 3 in a narrow phase interval of about 0.1.

5 DISCUSSION & CONCLUSIONS

We performed a detailed timing and broad-band pulse phase-resolved spectral analysis of the two *Suzaku* observations of the HMXB transient pulsar 1A 1118-61 during its 2009 giant outburst in its peak (Obs-1) and declining phase (Obs-2). Owing to the broad-band capability and high sensitivity of *Suzaku*, we have been able to investigate the complex energy dependence of the pulse profiles in more detail and in narrow energy bins compared to the previous works. In addition, we have detected a soft-excess peak (in the 0.3–2 keV range) at the main dip of the pulse profiles for both observations. Broad-band spectral analysis of the *RXTE* observations have been performed by Doroshenko et al. (2010), Devasia et al. (2011a) & Nespoli & Reig (2011) who reported the presence of a CRSF at ~ 55 keV. Suchy et al. (2011) performed broad-band spectral analysis of the same *Suzaku* observations using partial covering cutoff power law and compTT models and confirmed the presence of the CRSF

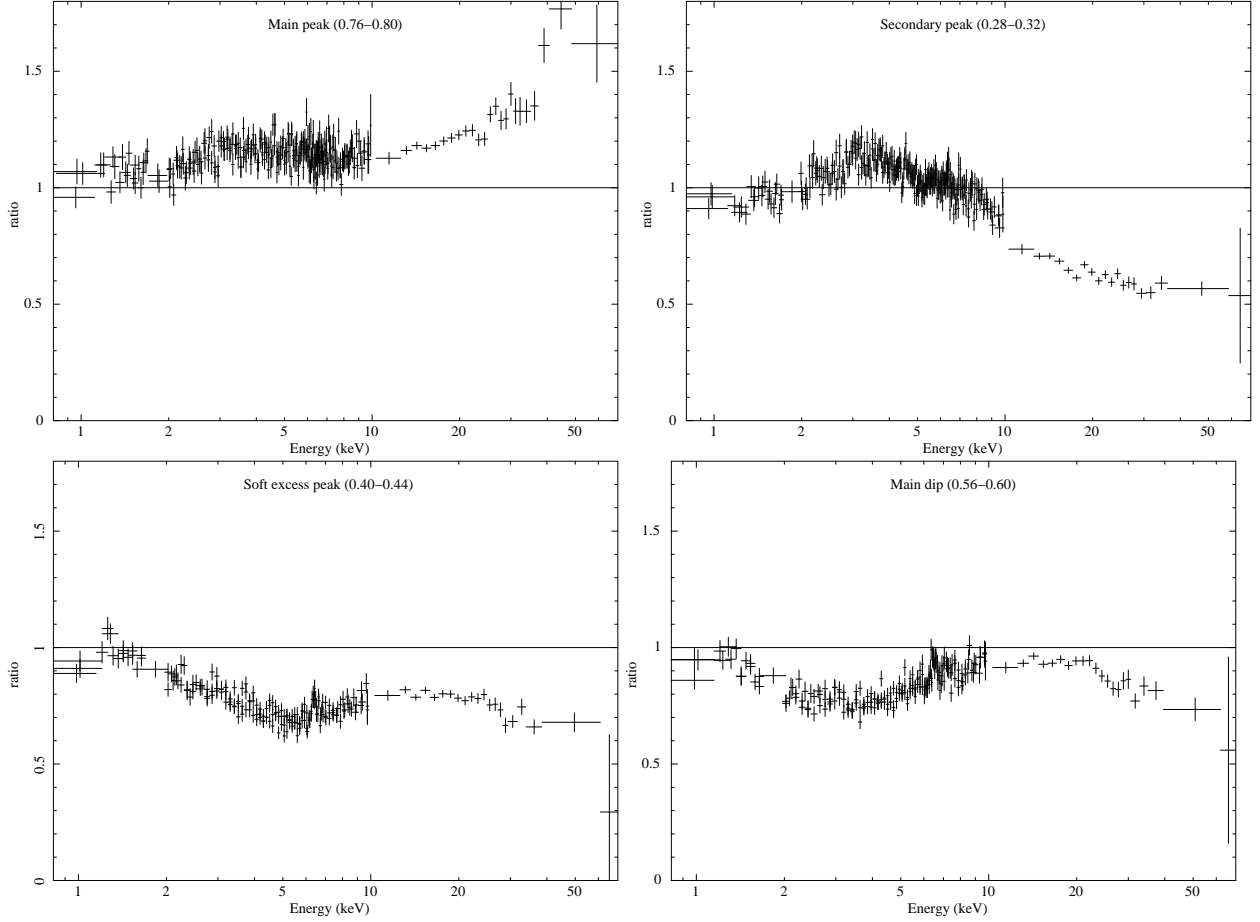


Figure 6. Phase-resolved to phase averaged spectral ratios for some particular phase bins (see values in parentheses) at the peak of the outburst on 15 January 2009 (Obs-1).

feature at ~ 55 keV, discussing also the possibility of the presence of a first harmonic at ~ 110 keV. Suchy et al. (2011) also included pulse phase-resolved analysis in three phase bins in the two peaks and in the minima of the pulse profiles where they reported some variations in the continuum and the centroid of the cyclotron line with pulse phase. We carried out a more detailed phase-resolved spectral analysis of the *Suzaku* observations in narrow phase bins using a partial covering cutoff power law model. Since the aim of the paper is to mainly investigate the variations of the spectral parameters with the pulse phase, we have not included GSO data in our analysis as the data quality is not suitable to perform phase-resolved analysis in narrow phase bins. We, therefore, cannot investigate the possible presence of a harmonic at ~ 110 keV. Variations of the CRSF parameters over the pulse phase are brought out very clearly in this source, and both the energy and the depth of the CRSF shows some interesting patterns of variation with pulse phase.

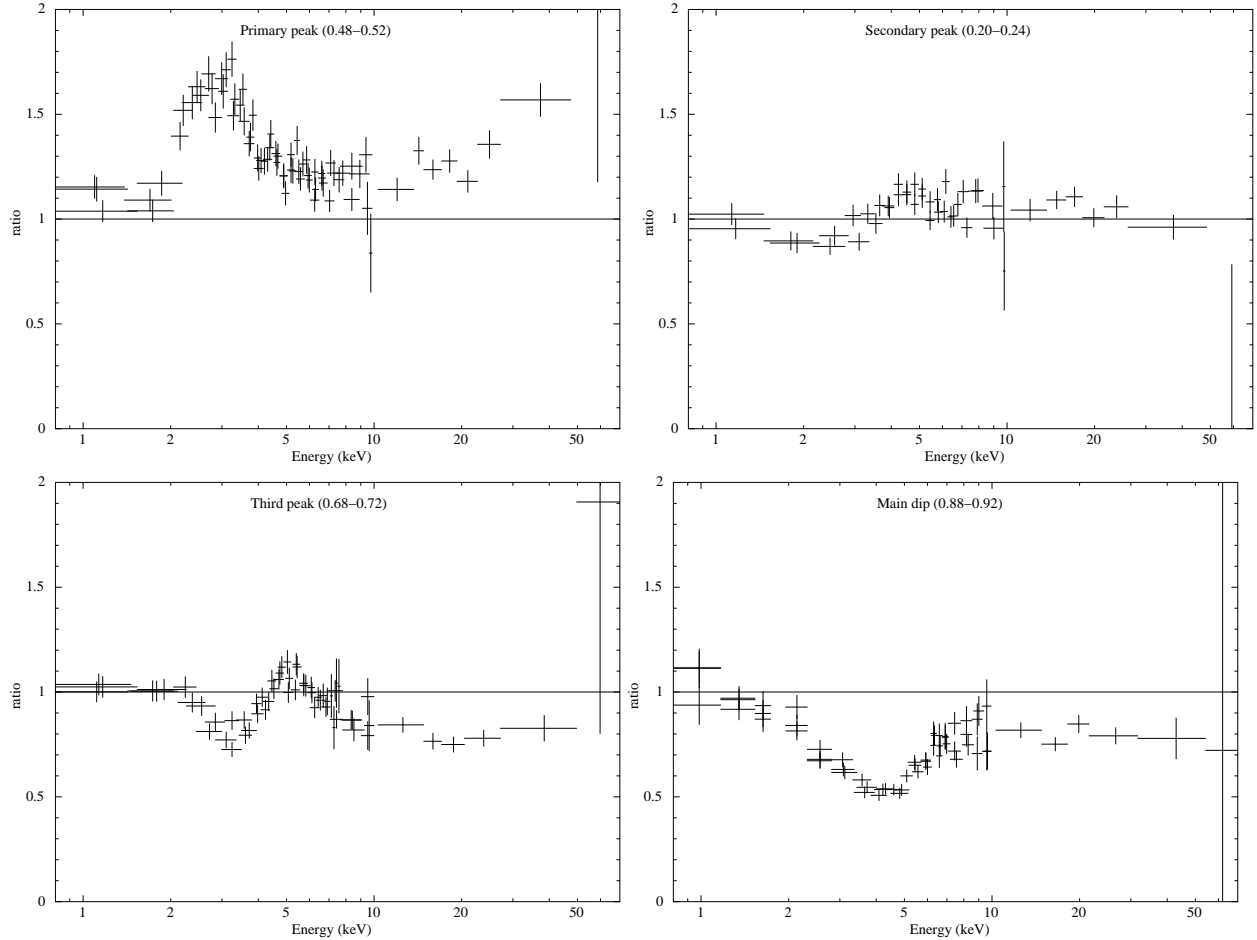


Figure 7. Same as Figure 6 but now for Obs-2.

5.1 Pulse Profiles: Energy Dependence & Soft-Excess Peak

Energy dependence of the pulse profiles have been found previously in other accretion powered X-ray pulsars such as 4U 0115+63 (Tsygankov et al. 2007) and Her X-1 (Nagase 1989). The energy dependence of the pulse profiles of the Be HMXB pulsar 1A 1118-61 during its 2009 outburst shows a multi peaked structure below ~ 10 keV, and a single asymmetric peak thereafter. These features have been reported previously using *RXTE* observations by Doroshenko et al. (2010), Devasia et al. (2011a), and Nespoli & Reig (2011). Owing to the better energy resolution, and the broader energy coverage, especially below 3 keV, the *Suzaku* data show a more detailed and clearer picture of the energy dependence of the pulse profiles. Suchy et al. (2011) analyzed *Suzaku* data using much wider energy bins than ours to probe the energy dependence. The presence of dips in the pulse profiles can be explained due to the presence of an additional absorption component at that pulse phase which obscures the radiation (Galloway et al. 2001). Recently similar energy dependence of the pulse profiles have also been found in other HMXB pulsars for example in GRO J1008-57 (Naik et al.

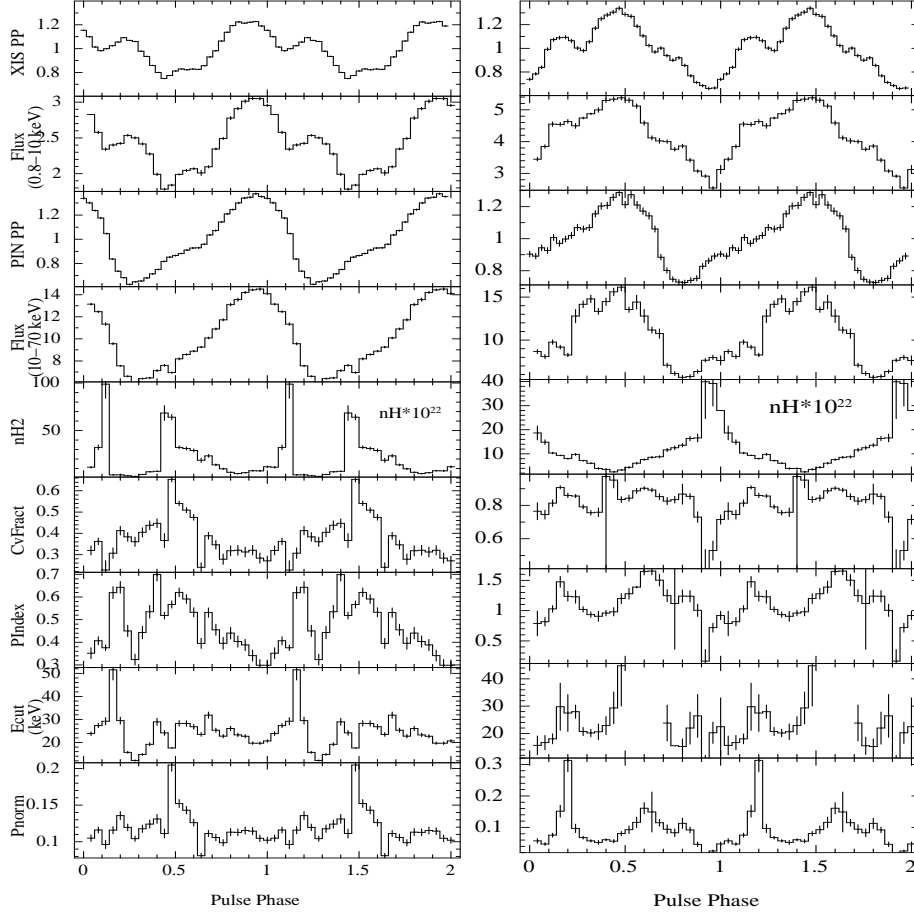


Figure 8. Variation of the spectral parameters with phase along with the pulse profile in the 0.2–12 keV range (obtained from XIS data; top panels), source flux in the 0.8–10 keV range (second panels from top), pulse profile in the 10–70 keV range (obtained from PIN data; third panels from top) and source flux in the 10–70 keV range (fourth panels from top). The left panels show the variation of the spectral parameters with pulse phase for Obs-1 and the right panels show the same for Obs-2. The units of flux and $nH2$ (equivalent hydrogen column density) are in $10^{-09} \text{ erg cm}^{-2} \text{ s}^{-1}$ and $10^{22} \text{ atoms cm}^{-2}$, respectively. Power-law normalization $Pnorm$ is in units of photons $\text{keV}^{-1} \text{ cm}^{-2} \text{ s}^{-1}$ at 1 keV

2011), and GX 304-1 (Devasia et al. 2011b), where the presence of the dips in the pulse profiles could be explained due to the presence of additional absorption component at those phases.

We have detected a soft excess peak in the lowest energies (0.3–2 keV range) at the main dips of the pulse profiles for both observations. A soft excess emission is common among accretion powered pulsars that have a low line of sight absorption (Paul et al. 2002; Hickox, Narayan, & Kallman 2004). The presence of a soft excess in accreting X-ray pulsars can be explained as by reprocessing in the thick magnetosphere shell (Mc Cray et al. 1982) or in the accretion column. The soft-excess could also be due to the reprocessing of the hard X-rays by the optically thick material in the inner edge of the accretion disk (Endo et al. 2000; Ramsay et al. 2002). In this work, fitting a blackbody component to the spectra of the phases corresponding to the soft excess peaks, we derived the radius of the soft excess emitting regions to be $\sim 6 \text{ km}$

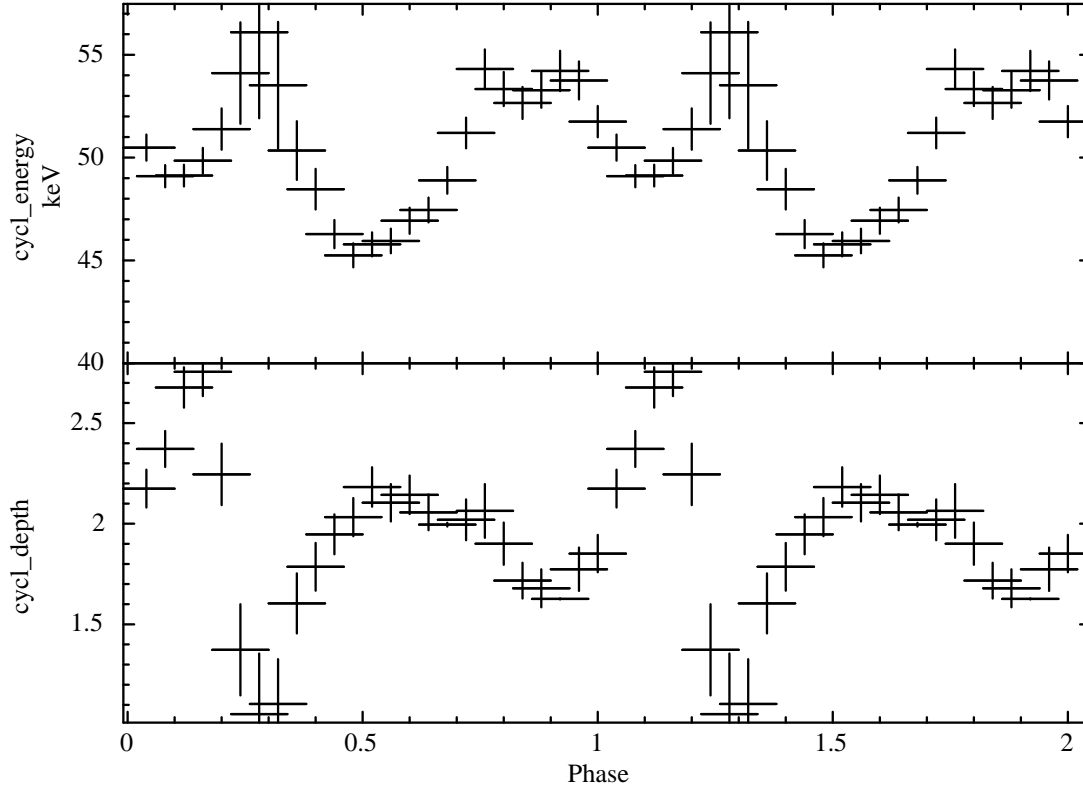


Figure 9. Variation of the cyclotron energy and depth with the pulse phase for Obs-1. Only 8 of the 25 points are independent. *cycl_energy* denotes the energy of the centroid of the CRSF feature & *cycl_depth* denotes the depth of the feature.

and ~ 4 km for Obs-1 and Obs-2 respectively. The small radii in both the cases suggest that the soft excess is being produced in the accretion mound itself or as reprocessed emission from the accretion column. Its origin from the inner accretion disk is very unlikely since the size of the emission region is very small compared to the inner disc radius which is of a few hundred kms. Also, the soft excess produced by the reprocessed disc blackbody component is usually seen over a broad phase range in other pulsars (Paul et al. 2002; Naik & Paul 2004) and not confined to a narrow phase range like in this source. .

5.2 Quasi Periodic Oscillations

The results related to the QPO feature found at 0.087 ± 0.009 Hz is almost similar to the one found by Devasia et al. (2011a) including its energy dependence. If the broad feature at 0.026 ± 0.003 Hz detected in Obs-2 is interpreted as being a QPO, assuming the generation of the QPO at the inner radius of the accretion disc, the decrease in the QPO frequency is consistent with the decrease in one order of magnitude of X-ray luminosity from Obs-1 to Obs-2 ($\nu_{qpo} \propto L_x^{3/7}$). Using this argument, the inferred value of the magnetic field is also in agreement with the one found by the CRSF (Devasia et al. 2011a). The quality factor of

the QPO feature in Obs-2 is however very low compared to the values found for the other accretion powered pulsars.

5.3 Pulse Phase averaged Spectroscopy

The strong and complex energy dependence of the pulse profiles bring out the requirement of a multicomponent model to fit the energy spectra of 1A 1118-61. Some of the continuum models that have been used extensively to describe the spectra successfully are the Negative & Positive powerlaws with a common Exponential (NPEX) continuum model (Mihara 1995; Makishima et al. 1999; Terada et al. 2006; Naik et al. 2008) and power-law with smooth Fermi-Dirac cutoff energy (Tanaka 1986). The partial covering absorption model (Endo et al. 2000; Mukherjee & Paul 2004) which consists of two power-law continua with a common photon index but different absorption components also describes the spectrum of these sources well. We had initially tried to fit the data with a partial covering model with a high-energy cutoff, but the spectra in some phases had a very low value of cutoff energy ($\sim 0-3$ keV) which is equivalent to a cutoff power-law model. The phase averaged data was thus well fitted with a partial covering cutoff power law model. The spectrum was softer and steeper at the declining phase of the outburst similar to what was found in some other HMXB transients like V 0332+53 (Mowlavi et al. 2006) and A 0535+26 (Caballero 2009). A narrow Iron $K\alpha$ line centered around 6.4 keV was detected in both observations which implied the presence of neutral or weakly ionized Iron. The possible origin of the iron line is the accretion disk or the circumstellar material, or the cool dense matter in the magnetosphere which reprocesses the emission.

The presence of the CRSF feature in the spectra had been reported previously by Doroshenko et al. (2010), Nespoli & Reig (2011), & Suchy et al. (2011). From the spectral fitting with Lorentzian profiles, we found that the CRSF line centers at 49 ± 0.5 and $52^{+4.9}_{-3.1}$ keV for Obs-1 and Obs-2 respectively. The best fitting centroids for Obs-1 and Obs-2 are consistent within confidence limits. The result is also consistent with a slight increase in the centroid energy with decreasing luminosity which is in agreement with the variation of the cyclotron line energy with that of the height of the accretion column. Higher the luminosity, lower in energy is the CRSF produced. This is because, higher luminosity implies higher accretion rate and a higher height for the accretion column. The CRSF feature is thus produced further away from the surface of the neutron star (Mihara et al. 2004; Nakajima et al.

2006). The CRSF feature is also broader in Obs-1 which may be due to the superposition of CRSF features produced in scattering regions at different heights of the accretion column which is higher in this case than in Obs-2.

5.4 Pulse Phase resolved spectroscopy

In addition to pulse phase averaged spectroscopy, we have performed pulse phase-resolved spectroscopy to understand the complex energy dependence of the pulse profiles. The column density of the material local to the neutron star (N_{H2}) of $\sim 10^{24} \text{ atoms cm}^{-2}$ can explain the dips seen in the pulse profiles. The changes in the value of N_{H2} and the covering fraction with pulse phase give us an idea about the properties of the plasma in the accretion stream. The plasma may be a clumpy structure with different values of opacity and optical depth. We find that the accretion column in Obs-1 represents a more clumpy structure with the dip at phase ~ 0.1 having a very high value of N_{H2} ($\sim 10^{24} \text{ atoms cm}^{-2}$) but a low covering value (~ 0.4). However, both values remain high in the main dip. Further, the accretion column in Obs-2, shows a more symmetric distribution of matter with a more or less constant value of covering fraction throughout the pulse phase.

The spectral hardening at the peaks of the pulse profile in Obs-1 may represent the passage of the magnetic axis through our line of sight, and a deep and a more direct view into the emission region along the magnetic axis (Pravdo et al. 1976). Similar regions of pulse hardening have been observed previously in other sources like Her X-1 (Pravdo et al. 1977, 1978), 4U 0115+63 (Johnston et al. 1978; Rose et al. 1979), & GX 1+4 (Doty, Hoffman & Lewin 1981).

Another feature that has been found is the variation of the CRSF parameters with pulse phase. Since the cross section and the depth of the cyclotron scattering feature is thought to depend significantly on the viewing angle of the accretion column, the CRSF properties may change with the rotation of the neutron star, hence with pulse phase. A large variation of ~ 10 keV in the cyclotron energy and a factor of 3 variation in the depth could either imply the dipole geometry being viewed at different angles at different pulse phases, or a more complex underlying magnetic field structure. Fitting of this observed variation of the cyclotron parameters with phase with a detailed and suitable theoretical model can be used to infer the structure of the magnetic field around the neutron star and also put constraints

on its other parameters like the inclination between the magnetic and rotation axis etc. This is however beyond the scope of the present work.

ACKNOWLEDGMENTS

We thank the reviewer for a very extensive review with many specific suggestions that helped us to improve the paper. This research has made use of data obtained through the High Energy Astrophysics Science Archive Research Center On line Service, provided by NASA/Goddard Space Flight Center.

REFERENCES

- Barnard J. J., Arons J., 1981, BAAS, 13, 851
- Brainerd J.J., Meszaros P., 1991, ApJ, 369, 179
- Caballero I., 2009, Ph.D thesis, IAAT University of Tuebingen
- Chevalier C., Ilovaisky S. A., 1975, IAU Circ, 2778, 1
- Coburn W., Heindl W. A., Rothschild R. E., 2002, ApJ, 580, 394
- Coe M. J., Payne B. J., 1985, Ap&SS, 109, 175
- Coe M. J., et al., 1994, A&A, 289, 784
- Corbet R. H. D., Peele A. G., 2000, ApJ, 530, L33
- Davidson K., Ostriker J. P., 1973, ApJ, 179, 585
- Devasia J., James M., Paul B., Indulekha K., 2011a, MNRAS, 414, 1023
- Devasia J., James M., Paul B., Indulekha K., 2011b, arXiv, arXiv:1106.3251
- Doroshenko V., Suchy S., Santangelo A., Staubert R., Kreykenbohm I., Rothschild R., Pottschmidt K., Wilms J., 2010, A&A, 515, L1
- Doty J. P., Hoffman J. A., Lewin W. H. G., 1981, ApJ, 243, 257
- Endo T., Nagase F., Mihara T., 2000, PASJ, 52, 223
- Eyles C. J., Skinner J. K., Willmore A. P., Rosenberg F. D., 1975, Nat, 342, 775
- Galloway D. K., Giles A. B., Wu K., Greenhill J. G., 2001, MNRAS, 325, 419
- Gnedin Yu. N., Sunyaev R. A., 1973, A&A, 25, 233
- Hickox R. C., Narayan R., Kallman T. R., 2004, ApJ, 614, 881
- Ives J. C., Sanford P. W., Bell Burnell S. J., 1975, Nat, 254, 578
- Janot-Pacheco E., Ilovaisky S. A., Chevalier C., 1981, A&A, 99, 274
- Johnston M., Bradt H., Doxsey R., Gursky H., Schwartz D., 1978, ApJ, 233, L71

- Koyama K, et al. , 2007, PASJ, 59, 23
- Lamb F. K., Pethick C. J., Pines D., 1973, ApJ, 184, 271
- Leyder J. C., Walter R., Lubinski P., 2009, ATel, 1949, 1
- Makishima K., Mihara T., Nagase F., Tanaka Y., 1999, ApJ, 525, 978
- Mangano V, 2009, ATel, 1896, 1
- Marashi L., Huckle H. E., Ives J. C., Sanford P. W., 1976, Nat, 263, 34
- Mc Cray R. A., Shull J. M., Boynton P. E., Deeter J. E., Holt S. S., White N. E., 1982, ApJ, 262, 301
- Meszaros P., Nagel W., 1985a, ApJ, 299, 138
- Meszaros P., Nagel W., 1985b, ApJ, 298, 147
- Mihara T., 1995, Ph.D. thesis, Univ. Tokyo
- Mihara T., Makishima K., Nagase F., 2004, ApJ, 610, 390
- Mitsuda K., et al. 2007, PASJ, 59, 1
- Motch C., Pakull M. W., Janot-Pacheco E., Mouchet M., 1988, A&A, 201, 63
- Mowlavi N., et al., 2006, A&A, 451, 187
- Mukherjee U., Paul B., 2004, A&A, 427, 567
- Nagase F., 1989, PASJ, 41, 1
- Nagel W., 1981a, ApJ, 251, 288
- Nagel W., 1981b, ApJ, 251, 278
- Naik S., Paul B., 2004, A&A, 418, 655
- Naik S., Callanan P. J., Paul B., Dotani T., 2006, ApJ, 647, 1293
- Naik S., et al., 2008, ApJ, 672, 516
- Naik S., Paul B., Kachhara C., Vadawale S. V., 2011, MNRAS, 413, 241
- Nakajima M., Mihara T., Makishima K., Niko H., 2006, ApJ, 646, 1125
- Nespoli E., Reig P., 2011, A&A, 526, A7
- Paul B., Nagase F., Endo T., Dotani T., Yokogawa J., Nishiuchi M., 2002, ApJ, 579, 411
- Paul B., Naik S., 2011, arXiv, arXiv:1110.4446
- Pravdo S. H., Becker R. H., Boldt E. A., Holt S. S., Serlemitsos P. J., Swank J. H., 1976, BAAS, 8, 512
- Pravdo S. H., Becker R. H., Saba J. R., Serlemitsos P. J., 1977, IAU Circ, 3116, 2
- Pravdo S. H., Bussard R. W., Becker R. H., Boldt E. A., Holt S. S., Serlemitsos P. J., 1978, ApJ, 225, 988
- Pringle J. E., Rees M. J., 1972, A&A, 21, 1

- Ramsay G., Zane S., Jimenez-Garate M. A., den Herder J.-W., Hailey C. J., 2002, MNRAS, 337, 1185
- Reig P., 2011, Ap&SS, 332, 1
- Rose L. A., Marshall F. E., Holt S. S., Boldt E. A., Rothschild R. E., Serlemitsos P. J., Pravdo S. H., Kaluzienski L. J., 1979, ApJ, 231, 919
- Staubert R., Pottschmidt K., Doroshenko V., Wilms J., Suchy S., Rothschild R., Santangelo A., 2011, A&A, 527, A7
- Suchy S., et al., 2011, ApJ, 733, 15
- Takahashi T., et al. 2007, PASJ, 59, 35
- Tanaka Y., 1986, in IAU Coll. 89, Radiation Hydrodynamics in Stars and Compact Objects, ed. Mihalas D. & Winkler K. H. (Heidelberg:Springer)
- Terada Y., et al., 2006, ApJ, 648, L139
- Tsygankov S. S., Lutovinov A. A., Churazov E. M., Sunyaev R. A., 2007, Astronomy Letters, 33, 368
- White N. E., Swank J. H., Holt S. S., 1983, ApJ, 270, 711